IOPscience iopscience.iop.org

Home Search Collections Journals About Contact us My IOPscience

Interaction between surface morphology and misfit dislocations as strain relaxation modes in lattice-mismatched heteroepitaxy

This article has been downloaded from IOPscience. Please scroll down to see the full text article.

2002 J. Phys.: Condens. Matter 14 12829

(http://iopscience.iop.org/0953-8984/14/48/323)

View the table of contents for this issue, or go to the journal homepage for more

Download details:
IP Address: 171.66.16.97
The article was downloaded on 18/05/2010 at 19:13

Please note that terms and conditions apply.

INSTITUTE OF PHYSICS PUBLISHING JOURNAL OF PHYSICS: CONDENSED MATTER

J. Phys.: Condens. Matter **14** (2002) 12829–12841 PII: S0953-8984(02)54034-0

Interaction between surface morphology and misfit dislocations as strain relaxation modes in lattice-mismatched heteroepitaxy

R Hull[1], J Gray[1], C C Wu[1], S Atha[1] and J A Floro[2]

[1] Department of Materials Science, University of Virginia, 116 Engineers Way, Charlottesville, VA 22902, USA
[2] Sandia National Laboratories, Albuquerque, NM 87185-1415, USA

E-mail: hull@virginia.edu

Received 27 September 2002
Published 22 November 2002
Online at stacks.iop.org/JPhysCM/14/12829

Abstract
We show how strained layer heteroepitaxial systems can serve as model systems for the study of dislocation energetics and kinetics in semiconductors through the introduction of strain-relieving misfit dislocation arrays. Such structures allow fundamental dislocation properties to be studied at carefully controlled stresses in the range 10^7–10^9 Pa. A parallel strain relaxation mode in strained heterostructures is via coherent islanding or surface roughening of the epitaxial layer. This mechanism acts both in competition and in cooperation with injection of misfit dislocations, and provides a further degree of control for study of the fundamental energetic and kinetic properties of dislocations. Using ultra-sensitive *in situ* wafer curvature measurements of stress during molecular beam epitaxy growth of Ge_xSi_{1-x}/Si heterostructures, the relative contributions of surface roughening and dislocation injection to strain relaxation may be qualitatively and quantitatively assessed. In addition, a new strain-stabilized morphology, 'quantum fortresses', comprising cooperative island nucleation around shallow strain-relieving pits, is identified during $Ge_{0.3}Si_{0.7}$/Si(100) heteroepitaxy. This configuration has potential application to nanoelectronic device architectures.

(Some figures in this article are in colour only in the electronic version)

1. Introduction

Epitaxial heteroepitaxial semiconductor structures have been central to a broad range of fundamental advances in our understanding of the properties of matter (for example the quantum Hall effect, interfacial electron transport, resonant tunnelling...) and are critical to the operation of multiple classes of electronic and optoelectronic devices (such as laser

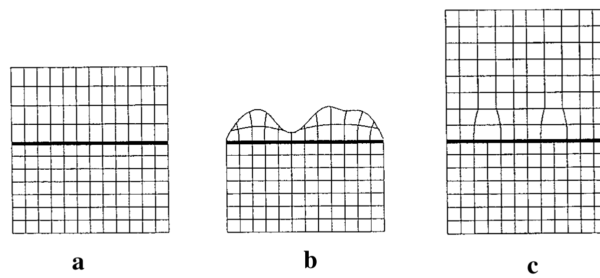

Figure 1. Mechanisms for strain accommodation/relief in lattice-mismatched heteroepitaxy: (a) elastic accommodation through tetragonal distortion of the epilayer unit cell, (b) epilayer surface roughening, (c) injection of interfacial misfit dislocations.

diodes, ultra-high-speed transistors and high-sensitivity optical detectors). The development of crystal growth techniques such as molecular beam epitaxy (MBE) and chemical vapour deposition (CVD) has enabled such heterostructures to be grown layer by layer, with atomic-scale precision. Nature has provided only a relatively small subset of semiconductor materials with matched or closely matched lattice parameters, and an even smaller subset with lattice parameters that match closely to crystals that can be successfully grown as large-diameter single-crystal substrates. Thus many epitaxial semiconductor material combinations of scientific and engineering importance employ components with substantially different lattice parameters. This induces very large strains and stresses in the epitaxial deposits that can relax through a set of mechanisms, the most important of which, at practical crystal growth and processing temperatures are shown in figure 1:

(a) The lattice mismatch strain can be accommodated by a tetragonal distortion of the unit cell in the epitaxial layer, whereby the in-plane layer lattice parameter is forced to that of the substrate, and the out-of-plane lattice parameter distorts[3] according to the Poisson effect. This creates a very high biaxial stress in the epitaxial layer, given by linear isotropic elasticity as:

$$\sigma_o = 2G\varepsilon(1+\nu)/(1-\nu). \tag{1}$$

Here G is the epilayer shear modulus, ν is the Poisson ratio of the epilayer and ε is the epitaxial layer strain, given by[4] $(a_e - a_s)/a_e$. For a lattice mismatch strain of 0.01 and elastic constants typical of diamond cubic and zincblende semiconductors, this gives lattice mismatch stresses of the order of 1–2 GPa. Such enormous stresses can be supported only in the limits of very thin films and low growth temperatures, as described below.

(b) The net stress/strain in the film can be reduced by roughening of the epitaxial film surface. For the situation where $a_e > a_s$, as is the case for the majority of widely studied epitaxial semiconductor systems, this will produce regions of dilation of the surface lattice parameter (with respect to a uniform planar film) at the waveform peaks and compression at the waveform troughs. This is illustrated in the finite element calculation of figure 2. The resultant laterally varying surface strain/stress field may then induce compositional segregation on the growing epitaxial surface—for example in the

[3] It increases with respect to its free lattice parameter for an epitaxial layer lattice parameter, a_e, greater than the substrate lattice parameter, a_s, and decreases for $a_e < a_s$.

[4] Note the usual convention in the strained layer epitaxy field is to define compressive strains/stresses in the epitaxial layer as positive, tensile strains/stresses as negative. Note also that many texts give a_s in the numerator, but the expression quoted here is rigorously correct for strain in the epitaxial layer (the difference between using a_e or a_s in the denominator will make only a very small correction for lattice parameter difference of order a few per cent).

Ge_xSi_{1-x}/Si(100) system, Ge atoms would be expected to be preferentially incorporated at the waveform peaks, where their larger bond length is more easily accommodated, and Si at the troughs.

The development of such surface morphology and compositional segregation requires sufficient adatom mobility of the deposited species on the growth surface. Thus the tendency for such roughening increases with increasing growth temperature and decreasing growth rate, as well as with increasing strain. For sufficiently high surface mobility, the film may grow as a series of discrete clusters. This evolution has been extensively studied in the Ge/Si(100) system, and it is observed that at growth temperatures greater than about 500 °C (depending also on the growth rate), epitaxial growth follows the Stranski–Krastanov mode, whereby a thin planar wetting layer of a few monolayers of Ge forms first, and then pseudomorphic (i.e. dislocation-free) islands form upon the wetting layer [1]. The morphological evolution of these strained clusters with increasing amount of deposited Ge has been shown to first correspond to pseudomorphic 'hut clusters' with {510} faces, then to the formation of higher aspect ratio pseudomorphic 'domes' with predominant {311} facets, and then to dislocated domes [2–5]. For dilute Ge_xSi_{1-x} alloys on Si(100), the morphological evolution shows a similar set of transitions [6], provided that the growth temperature (e.g. $\geqslant$700 °C for $x = 0.2$) is high enough to overcome kinetic limitations preventing the surface from reaching its equilibrium state. The length scales for the transitions also increases with a scaling factor in the range ε^{-1}–ε^{-2} [6–8]. Lower growth temperatures can lead to markedly different morphologies, as will be illustrated later in this paper.

(c) Another prevalent mechanism for strain relaxation in thicker epitaxial layers is the introduction of misfit dislocations, which as illustrated in figure 1(c) allows the epitaxial layer to relax towards its free lattice parameter. These dislocations comprise strain-relieving interfacial segments, terminated by 'threading arms' joining the interfacial segment to the epilayer surface. A minimum epitaxial layer thickness, the critical thickness $h_c(\varepsilon)$ [9], exists above which misfit dislocations are energetically favoured in the film. Above h_c, the strain energy relaxed in the film, E_a, more than compensates for the additional self-energy term associated with the dislocation strain field and core, E_T. The critical thickness is thus defined by equivalence of these energies, or their associated stress terms, σ_a, σ_T, yielding for $\sigma_a = \sigma_T$:

$$2G\cos\phi\cos\lambda(1+\nu)/(1-\nu) = Gb\cos\phi(1+\nu\cos^2\theta)\ln(\alpha h/b)/4\pi h(1-\nu). \qquad (2)$$

Here G is the epilayer shear modulus, ν is the epilayer Poisson ratio, h is the epilayer thickness, α is a factor describing the dislocation core energy, b is the magnitude of the dislocation Burgers vector, and ϕ, λ and θ are geometrical factors defining the orientations of the dislocation Burgers vector and slip plane. The locus of $h_c(\varepsilon)$ versus x in the Ge_xSi_{1-x}/Si(100) system is shown in figure 3.

Kinetic factors again play a major role in defining the rate of introduction of misfit dislocations. Activation barriers associated with the nucleation and propagation of misfit dislocations greatly limit the rate of evolution of the interfacial misfit dislocation array at lower growth rates and temperatures [10]. This means that epitaxial layers substantially greater than the equilibrium prediction may be grown before significant misfit dislocation densities are observed, as is illustrated for a growth temperature of 550 °C in the Ge_xSi_{1-x} system [11] in figure 3. A useful measure of the degree of metastability in the system is the excess stress, σ_{ex}, defined by Dodson and Tsao [12] as:

$$\sigma_{ex} = \sigma_a - \sigma_T. \qquad (3)$$

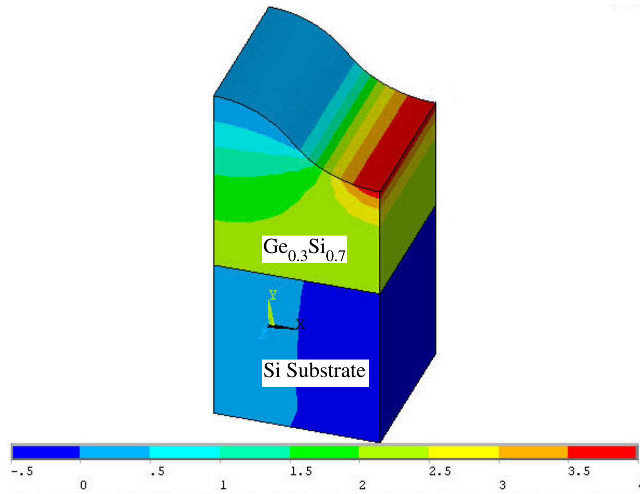

Figure 2. Finite element calculation using anisotropic elastic constants of the stress distribution (σ_{xx}, perpendicular to the sinusoidal modulations) in a $Ge_{0.3}Si_{0.7}$ film with a mean thickness of 100 nm and a one-dimensional sinusoidal surface modulation with an amplitude of 50 nm and a period of 200 nm. Stress contours are in GPa. The average epitaxial film stress in this calculation is 1.01 GPa. The corresponding film stress in a 100 nm planar $Ge_{0.3}Si_{0.7}$ film is 2.11 GPa. Calculations were performed on ANSYS 5.7.

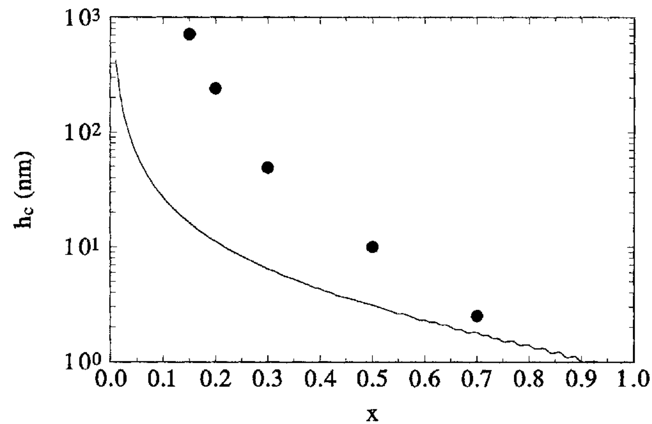

Figure 3. Critical thickness in the Ge_xSi_{1-x}/Si(100) system, calculated from the Matthews–Blakeslee equilibrium theory [9]. Also shown are experimental data (solid circles) from Bean *et al* [11] for a growth temperature of 550 °C.

The magnitude of strain relaxation by misfit dislocations then follows the form:

$$\Delta\varepsilon(t) \sim \int N(\sigma_{ex}) \exp(-E_N/kT) V(\sigma_{ex}) \exp(-E_v/kT)\, \mathrm{d}t. \tag{4}$$

Here E_N and E_v are the activation energies for dislocation nucleation and glide respectively, with $N(\sigma_{ex})$ and $V(\sigma_{ex})$ the corresponding prefactor terms which are functions of the excess stress driving dislocation motion in the system. The integral is evaluated over all time for which $\sigma_{ex} > 0$ for either a growth or annealing cycle. Detailed expressions exist for dislocation glide velocities in the Ge_xSi_{1-x}/Si system [13–16], as illustrated by figure 4. However,

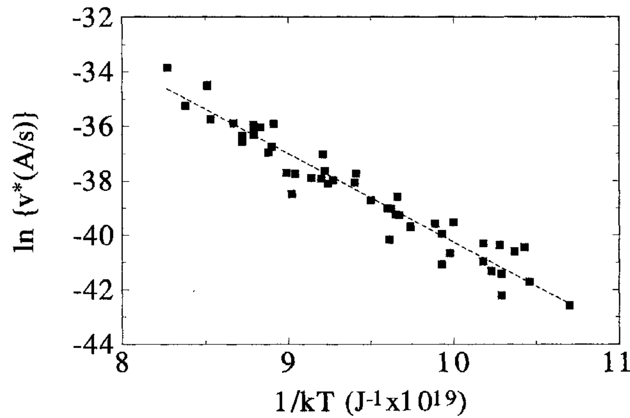

Figure 4. Measured (by *in situ* transmission electron microscopy) misfit dislocation glide velocities in the Ge_xSi_{1-x}/Si(100) system [14], normalized to equivalent velocities, v^*, at a stress of 1 Pa in pure Si using the equation $v = \exp[v_o]\sigma_{ex}\exp[-(E_v - 0.6x)/kT]$, where v is the measured dislocation velocity and the expression $(E_v - 0.6x)$ is in eV. The linear fit to the experimental data using this equation is given by $v_o = -7.8 \pm 1.4$ and $E_v = 2.03 \pm 0.10$ eV.

corresponding expressions for dislocation nucleation do not exist, due to the existence of different nucleation mechanisms (heterogeneous, homogeneous and multiplication) in different regimes of epilayer thickness, strain and growth temperature [10, 17].

These different strain relaxation mechanisms (elastic distortion, surface roughening, and misfit dislocation injection) both compete and cooperate with each other during lattice-mismatched heteroepitaxy. For example, surface roughening reduces the overall epilayer strain available for dislocation injection, as illustrated by figure 2, thereby inhibiting that process, yet can also create local stress concentrators that locally enhance dislocation nucleation [18]. The competition between elastic accommodation of strain and dislocation injection is adequately described by the concepts of critical thickness and excess stress [9, 12], but the balance between surface roughening/islanding and dislocation injection is more complex. Mapping of the different regimes where each dominates has been approached both theoretically (e.g. [19]) and experimentally (e.g. [20]).

Despite these complexities, lattice-mismatched heteroepitaxy provides unique opportunities for the study of the fundamental properties of dislocations in semiconductors. The epitaxial film stress can be accurately controlled through the film thickness and composition, and can range from tens of MPa to more than 1 GPa. The length of the propagating dislocation threading arms, a crucial parameter in microscopic models of dislocation motion by kink nucleation and diffusion [13, 14, 21], is defined by the film thickness. The dislocation microstructure can be modified (e.g. through separation of the parent $a/2\langle 110\rangle$ dislocation into $a/6\langle 211\rangle$ partials in diamond cubic and zincblende semiconductors [14, 22]). Dislocation can be studied in films of alloy materials (e.g. Ge_xSi_{1-x} and $Ga_xIn_{1-x}As$) that are not readily available as bulk single crystals. Finally, as will be described in this paper, the ability to independently control surface morphology and dislocation injection provides significant new insight into these cooperative mechanisms.

2. Experimental details

In the experiments described in section 3, $Ge_{0.3}Si_{0.7}$ films were grown using MBE on (001) Si substrates [23, 24]. The 300 μm thick substrates were chemically cleaned and oxidized

using a modified Shiraki procedure [25] before being loaded into the growth chamber. The resulting surface oxide was desorbed at a temperature of 820 °C and a 1000 Å Si buffer layer was then grown at 750 °C. After buffer growth, the substrate temperature was lowered to the Ge_xSi_{1-x} growth temperature (550 °C for most of the results described here), and following a substantial pause (of the order of 1 h) to enable temperature equilibration for accurate wafer curvature analysis, a further 5 nm of Si buffer was grown followed by $Ge_{0.3}Si_{0.7}$ alloy growth. The base pressure in the chamber prior to growth was typically 2×10^{-10} Torr. Growth rates were controlled using calibrated quartz crystal monitors. The growth surface was monitored using reflection high-energy electron diffraction (RHEED). RHEED patterns obtained during Si buffer growth consisted of a Laue circle of sharp spots that indicates a smooth 2×1 reconstructed surface. The stress in the SiGe films was measured in real-time by using a multibeam optical stress sensor (MOSS) technique [6, 23, 24] that measures wafer curvature, R, with a detectable limit of several km radius of curvature, corresponding to the stress induced by one monolayer of Ge on a 300 μm Si(100) wafer, as determined by Stoney's formula:

$$1/R = 6\sigma_f h_f / M_s h_s^2. \quad (5)$$

Here, σ_f is the epilayer film stress, h_f the epilayer film thickness, h_s the substrate thickness, and M_s the substrate biaxial modulus.

The surface morphology of as-grown films was characterized *ex situ* using contact mode atomic force microscopy (AFM) on a Park Scientific Autoprobe AFM. Selected samples were also studied by transmission electron microscopy (TEM) using both plan view and cross-sectional modes on a JEOL 2000 FX TEM operated at 200 kV. For contacting to the quantum quadruplet structures illustrated in figure 12, an FEI 200 focused ion beam (FIB) with an energy of 30 keV, using a nominal spot size of 10 nm and a probe current of 1 pA, was employed. Beam-induced Pt deposition was from a methylcyclopentadieyl(trimethyl)platinum source.

3. Competitive and cooperative mechanisms of surface morphology and misfit dislocations

Using the *in situ* wafer curvature measurements described in section 2, we can continuously measure the net stress, σ_n, during growth of Ge_xSi_{1-x}/Si(100) films (for all results described in this section, $x = 0.3$). The total amount of stress relaxed, $\Delta\sigma_n$, will be given by the sum of the stress relaxed due to surface roughening, $\Delta\sigma_s$, and the stress relaxed due to misfit dislocation injection, $\Delta\sigma_d$:

$$\Delta\sigma_n = \Delta\sigma_s + \Delta\sigma_d. \quad (6)$$

The quantity $\Delta\sigma_d$ can be measured *ex situ* by TEM plan view measurements of dislocation density using the relation:

$$\Delta\sigma_d = b \cos\theta / p. \quad (7)$$

Here b is the magnitude of the dislocation Burgers vector (0.39 nm for $b = a/2\langle 110\rangle$ dislocations in diamond cubic $Ge_{0.3}Si_{0.7}$), θ is the angle between the interfacial dislocation line direction and its Burgers vector (60° for the (100) interface), and p is the average spacing between misfit dislocations.

Figure 5 shows the stress–thickness ($\sigma_n h$) product for the $Ge_{0.3}Si_{0.7}$ epilayer film during growth at 550 °C and a growth rate of 0.15 A s^{-1}. In common with all films studied at this composition, three distinct relaxation regimes were observed:

(I) A regime, under these growth conditions spanning epilayer thicknesses from 0–10 nm, where the surface is essentially planar, as evidenced by streaky RHEED patterns and subsequent AFM scans.

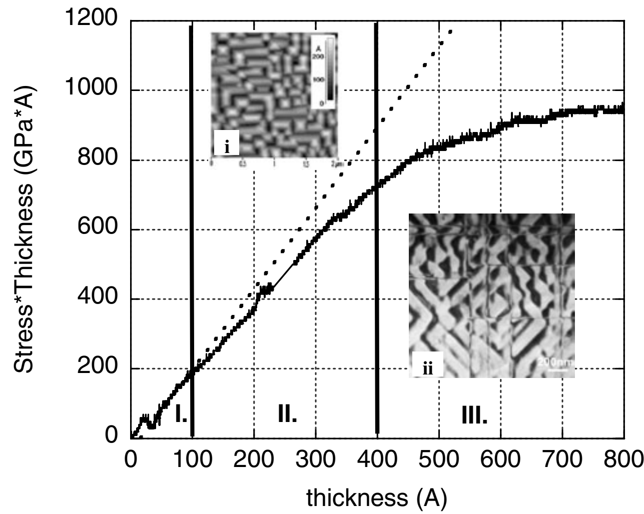

Figure 5. *In situ* wafer curvature measurements of the stress–thickness product during growth of a $Ge_{0.3}Si_{0.7}$/Si(100) film at a temperature of 550 °C and a growth rate of 0.15 A s^{-1}. Insets show (i) an AFM image of a 30 nm thick film and (ii) a TEM image of a 40 nm thick film.

(II) A regime, under these growth conditions spanning epilayer thicknesses from 10–40 nm, where there is considerable surface morphology, as evidenced by spotty RHEED patterns and subsequent AFM scans as in the inset (i) in figure 5. Typical relaxations of the net film stress, $\Delta\sigma_n/\sigma_n$, are of the order of 10%, as evidenced by the deviations of the measurements (solid line) from the trajectory for a fully stressed film ($\Delta\sigma_n = 0$, dotted line). In this regime, significant densities of misfit dislocations have not yet been introduced (i.e. $\Delta\sigma_d \sim 0$, $\Delta\sigma_n = \Delta\sigma_s$).

(III) A regime, under these growth conditions spanning epilayer thicknesses of 40 nm and greater, where substantial densities of misfit dislocations are introduced, as indicated by the inset TEM image (ii) in figure 5. Here, stress relaxation increases considerably with increasing epilayer thickness, $\Delta\sigma_n/\sigma_n$, of the order of several tens per cent, and all terms $\Delta\sigma_n$, $\Delta\sigma_s$ and $\Delta\sigma_d$ are non-zero.

Clearly the transition thicknesses between these different regimes depend critically upon the system kinetics, which at the fixed $Ge_{0.3}Si_{0.7}$ thickness and (100) interface orientation described here are defined by the growth rate and growth temperature of the epitaxial film. The latter is expected to dominate, as being a thermally activated process it depends exponentially upon growth temperature, whereas the effect of growth rate will be to introduce a linear dependence upon the time at a particular temperature required to reach a given epitaxial film thickness. Thus we would expect the overall magnitude of stress relaxation, $\Delta\sigma_n$, at a given epilayer thickness to increase with increasing growth temperature and decreasing growth rate. Similarly we would expect the transition thicknesses I $\rightarrow$ II and II $\rightarrow$ III to decrease with increasing growth temperature or decreasing growth rate. These anticipated trends are confirmed in figures 6 and 7.

The net stress relaxation $\Delta\sigma_n/\sigma_n$ is plotted versus film thickness for different growth temperatures and rates in figure 8. Again, it is observed that $\Delta\sigma_n/\sigma_n$ increases with increasing growth temperature and decreasing growth rate. Also shown are initial TEM plan view measurements of the relaxation component due to introduction of dislocations, $\Delta\sigma_d$. It is

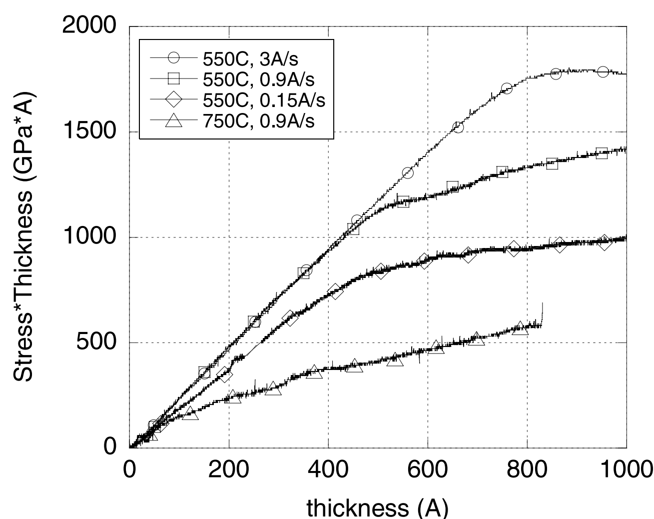

Figure 6. *In situ* wafer curvature measurements of the stress–thickness product during growth of $Ge_{0.3}Si_{0.7}$/Si(100) films as functions of temperature and growth rate.

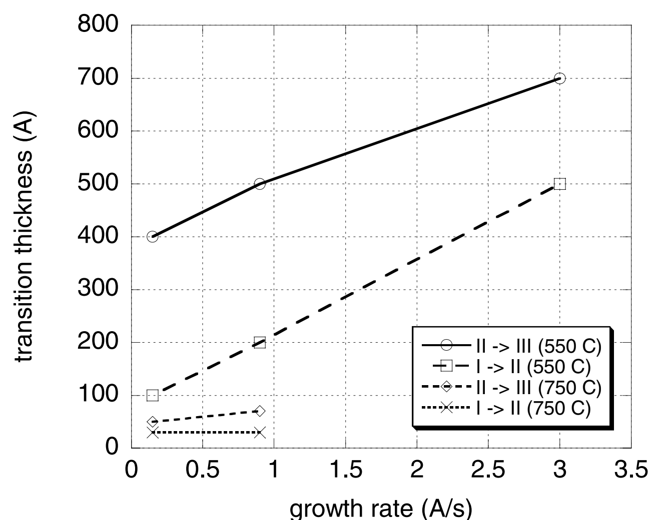

Figure 7. *In situ* wafer curvature measurements of the transition thicknesses between planar and roughened films (I $\rightarrow$ II) and undislocated to dislocated films (II $\rightarrow$ III) as functions of temperature and growth rate.

observed that the measured $\Delta\sigma_d \ll \Delta\sigma_n$, indicating that either there is a surprisingly dominant non-dislocation component to strain relaxation, i.e. the surface morphology term, $\Delta\sigma_s$, or that some other contribution is dominating. We are currently extending these preliminary measurements to quantitatively explore the relative contributions of $\Delta\sigma_n$, $\Delta\sigma_d$ and $\Delta\sigma_s$ as functions of film thickness, growth temperature and growth rate.

Under certain growth conditions we have discovered evolution of a complex surface morphology that is illustrated in figures 9 and 10. The evolution of this morphology is recorded in figure 9 for a growth temperature of 550 °C and a growth rate of 0.9 A s^{-1}.

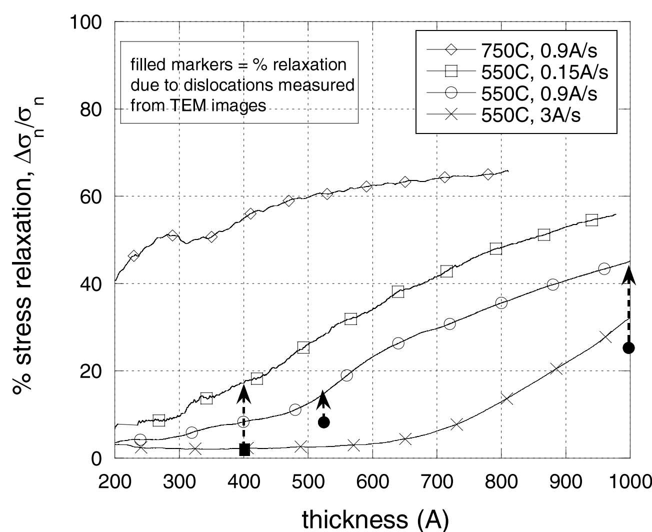

Figure 8. *In situ* wafer curvature measurements of the fractional relaxation of total film stress, $\Delta\sigma_n/\sigma_n$, as a function of film thickness, growth temperature and growth rate. Also shown are initial measurements of fractional stress relaxation due to misfit dislocation injection, $\Delta\sigma_d$.

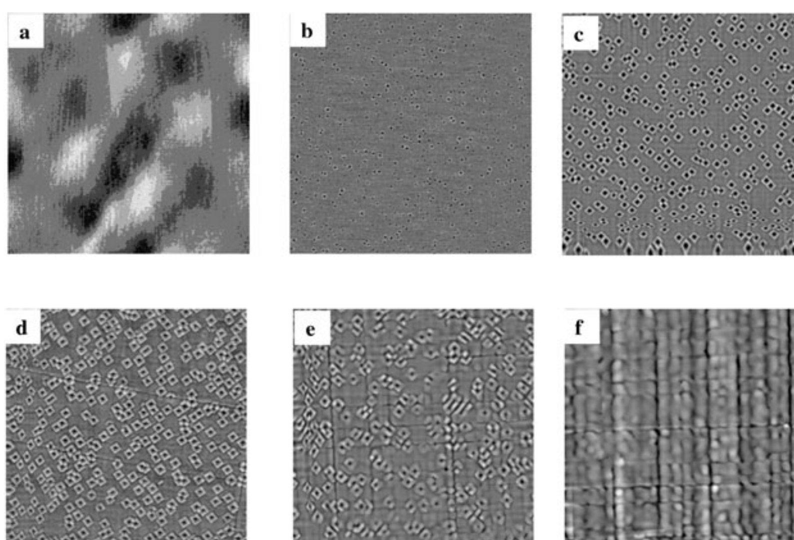

Figure 9. Evolution of the 'quantum fortress' surface morphology for growth of $Ge_{0.3}Si_{0.7}$/Si(100) at a growth temperature of 550 °C and a growth rate of 0.9 A s^{-1}. AFM scans are 5 μm × 5 μm in area. $Ge_{0.3}Si_{0.7}$ film thicknesses are (a) 0 nm, (b) 15 nm, (c) 30 nm, (d) 53 nm, (e) 100 nm and (f) 200 nm.

Following the growth of the Si buffer layer (9(a)), only a few ångstroms of surface roughness are observed. As the films grows, over film thicknesses of 5–15 nm (9(b)), a characteristic surface pit morphology evolves that is believed to be associated with strain relief [18, 26]. The pits have edges along ⟨010⟩ directions. At this stage, their depth is of the order of 1 nm while the width is approximately 50 nm, and they have sidewall angles of about 3°.

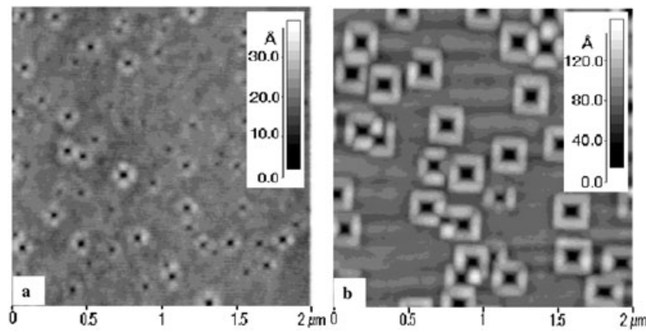

Figure 10. AFM images (2 μm × 2 μm) of $Ge_{0.3}Si_{0.7}$/Si(100) growth at 550 °C, 0.9 A s^{-1} for (a) 15 nm and (b) 30 nm film thicknesses showing quantum quadruplets and quantum fortresses. The darkest areas in the images correspond to pits, the lightest to islands.

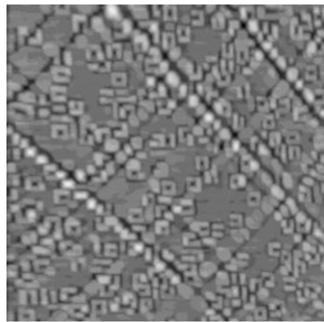

Figure 11. AFM image (5 μm × 5 μm) of 75 nm $Ge_{0.3}Si_{0.7}$/Si(100) growth at 550 °C, 0.9 A s^{-1} followed by 1 h 550 °C anneal.

As the film thickness increases, islands start to form on each edge of the pit perimeter (figures 9(b) and 10(a), epilayer thickness of 15 nm) to form quadruplets. As the film grows further, these islands extend to form continuous walls along the pit perimeter (figures 9(c) and 10(b), epilayer thickness of 30 nm). We call such structures 'quantum fortresses'. At this stage the pit depth has increased to about 10 nm and the pit width has doubled to about 100 nm. The sidewall angle of the pits has increased to 9°, which is close to that of the typical hut cluster island $\langle 501 \rangle$ facet [2]. The quantum fortress structures persist through the initial introduction of misfit dislocations (figures 9(d) at an epilayer thickness of 53 nm), but the dislocations do eventually, when their densities become sufficiently high, destabilize the quantum fortress structure, as is illustrated in figures 9(e) and (f) for epilayer thicknesses of 100 and 200 nm respectively. This is further borne out by the AFM image of figure 11, which shows a $Ge_{0.3}Si_{0.7}$ film grown to 75 nm under the same conditions and then annealed at 550 °C for 1 h to inject additional misfit dislocation line length into the interface. In this case, the quantum fortress morphology is destabilized close to the dislocations, and is only retained in regions far from dislocations where the epilayer strain field is relatively intact. In contrast, standard dome-shaped islands do form along the dislocation lines, where the strain relaxation fields will encourage the formation of Ge_xSi_{1-x} islands with a larger lattice parameter (compared to the Si substrate), as has been observed by Ross [27].

The quantum fortress morphology, while entirely reproducible over the range of conditions described below, is apparently stabilized by relatively localized (in T, t, ε space) kinetic and

strain-driven pathways. First, as described in the previous paragraph, it is stabilized by the film strain; as the strain disappears due to the introduction of misfit dislocations, so do the quantum fortresses. The morphology also appears in only certain regimes of growth temperature and growth rate. At 550 °C, we observe the fortresses at growth rates of 0.9 and 3.0 A s^{-1}, but not at 0.15 A s^{-1}. Thus it appears that if surface diffusion lengths are great enough, the fortress morphology does not form (instead we observe the standard hut cluster like morphologies observed in the inset (i) to figure 5 and described in [6]). With respect to growth temperature, it is found that at a fixed growth rate of 0.9 A s^{-1}, the fortress morphology is observed at 550 °C, but not at 350 or 750 °C. The destabilization with respect to higher growth temperature again indicates that higher surface diffusion lengths enable lower-energy surface microstructures to develop. The absence of the fortress microstructure at the lower growth temperature is simply a manifestation of the fact that at 350 °C the surface diffusion lengths are sufficiently low that the development of long-range cooperative microstructure is not possible. Thus, in conclusion, it is apparent that the quantum fortress morphology at the $Ge_{0.3}Si_{0.7}$ composition is a metastable state stabilized by strain and by limited surface diffusivity. Further studies are under way to explore fortress stability in greater detail as a function of growth temperature, growth rate and composition (strain).

A similar surface morphology has been previously reported in the Ge_xSi_{1-x}/Si(100) system, but in that case was induced by deliberate incorporation of C to produce silicon carbide precipitates that induce pit formation in the Si buffer layer, with subsequent cooperative nucleation of islands to surround the pits in the Ge_xSi_{1-x} heteroepitaxial film [28]. However, the quantum fortress morphology in our work appears to be intrinsically associated with the growth conditions and associated kinetically limited strain relaxation pathways. First, AFM analysis shows no evidence of any pit-like structures present on the silicon buffer surface immediately before growth of the Ge_xSi_{1-x} material. Furthermore, although we cannot rule out possible effects of C incorporation during Ge_xSi_{1-x} alloy growth, the fact that the pits do not trace back to the initial Ge_xSi_{1-x} growth interface, and the fact that no pitting is observed in the initial low-temperature (550 °C) Si layer, indicates that contamination at the growth interfaces is not the controlling factor in determining the subsequent quantum fortress morphology in our experiments.

Finally we note that this complex morphology, particularly in the precoalescence stage indicated in figure 10(a), has the same symmetry as that required for the concept of quantum cellular automata (QCA) [29] where additional electronic charges placed on an array of four quantum dots at the corners of a square assume bistable states according to electron occupation of the two pairs of opposite corners. This mimics the two states of digital logic and logic gates and more complex circuits have been proposed based upon this phenomenon [29]. Power-delay products/packing densities for such architectures can in principle be many orders of magnitude lower/higher than in conventional Si MOSFET circuits. Initial experimental proofs of concept have been fabricated [30], using Al/Al_2O_3 tunnel junctions, but the highest operating temperatures reported to date have been less than 1 K, due to the low energy difference between the bistable states at dimensions accessible using conventional lithographic techniques. The quantum fortress morphology (or at least its quadruplet precursor) offers the possibility of forming semiconductor QCA cells. The location of the initial pits may be programmable by lithographic seeding, and their sizes may be scaleable through epilayer thickness (as we already know) and composition (strain). Initial attempts are being made to electrically contact these structures, in collaboration with Snider and co-workers at the University of Notre Dame. Figure 12 shows preliminary results using FIB-induced deposition of Pt lines with line widths of about 70 nm (the advantage of FIB contacting is that we can visually align to the random site locations of the quadruplets).

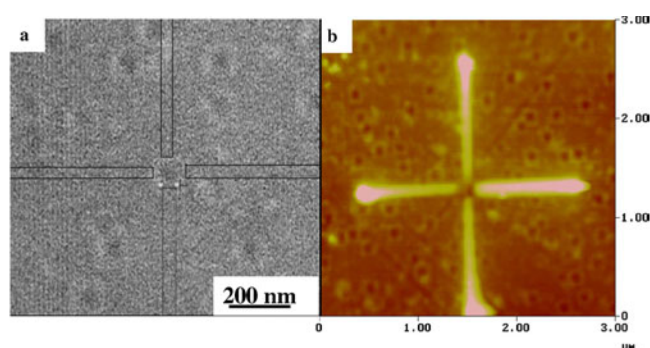

Figure 12. (a) Secondary electron image created by 30 keV Ga^+ FIB showing pit/quadruplet structures and the ability to visually align to the random site locations of the quadruplets (the capture of such an image removes less than one monolayer of material). (b) FIB-induced deposition of Pt contacts to individual quadruplet components at a beam current of 1 pA (nominal spot size 10 nm).

4. Conclusions

Strained layer heteroepitaxial films provide broad new opportunities for the study of fundamental properties of dislocations in semiconductors. In particular, in this paper, we have emphasized the qualitative and quantitative understanding of the relative roles of misfit dislocation injection and surface roughening in effecting strain relaxation in such structures. It is observed that during growth of $Ge_{0.3}Si_{0.7}$/Si(100) heterostructures three broad regimes of microstructure and strain relief are observed: an initial quasi-planar growth (regime I), followed by a transition to a highly non-planar morphology absent of misfit dislocations (regime II), followed by misfit dislocation injection (regime III). The magnitude of strain relaxation in each regime increases with increasing growth temperature and decreasing growth rate, consistent with an increased time–temperature cycle enhancing kinetically limited processes. Similarly, the transition thicknesses between regimes (I $\rightarrow$ II and II $\rightarrow$ III) decrease with increasing growth temperature and decreasing growth rate.

Over a limited range of growth conditions, a novel and complex surface microstructure is formed by a three-stage process with increasing thickness of the epitaxial layer:

(i) Square (sidewalls along $\langle 010 \rangle$), shallow pits form in the growing heteroepitaxial film as a strain relief mechanism.

(ii) Islands form on the edge of each pit to form a ‘quantum quadruplet’ structure.

(iii) The islands elongate along the wall edges to form a continuous ‘quantum fortress’ structure.

The quantum fortress structures are stabilized by strain, and selectively disappear when injection of misfit dislocations locally relaxes strain in the structure. They also appear to occur in a relatively narrow range of kinetic pathways, whereby higher growth temperatures and lower growth rates allow the structure to evolve towards more conventional (i.e. widely observed) surface microstructures. The symmetry of such structures may have application to novel nanoelectronic architectures such as quantum cellular automata.

Acknowledgments

The authors would like to acknowledge invaluable discussions with M Kammler, J Bean, T Vandervelde and P Kumar (UVa), F Ross and R Tromp (IBM) and G Snider (Notre Dame University). This work was funded by NSF-DMR primarily under the UVA-UIUC-IBM-Sandia Focused Research Group 'Nanoscale Morphological Evolution of Semiconductor Surfaces' (grant no 0075116), with partial support (SA) from the NSF-MRSEC at UVa, 'The Center for Nanoscopic Materials Design'. JAF was supported by the Division of Materials Science and Engineering, Office of Science, US Department of Energy. Sandia is a multiprogramme laboratory operated by Sandia Corporation, a Lockheed Martin Company, for the United States Department of Energy under contract no DE-AC04-94AL85000.

References

[1] Eaglesham D J and Cerullo M 1991 *Appl. Phys. Lett.* **58** 2276
[2] Mo Y-W, Savage D E, Swartzentruber B S and Lagally M G 1990 *Phys. Rev. Lett.* **65** 1020
[3] Tomitori M, Watanabe K, Kobayashi M and Nishikawa O 1994 *Appl. Surf. Sci.* **76/77** 322
[4] Ross F M, Tromp R M and Reuter M C 1999 *Science* **286** 1931
[5] Medeiros-Ribeiro G, Bratkovski A M, Kamins T I, Ohlberg D A A and Williams R S 1998 *Science* **279** 353
[6] Floro J A, Chason E, Freund L B, Twesten R D, Hwang R Q and Lucadamo G A 1999 *Phys. Rev.* B **59** 1990
[7] Tromp R M, Ross F M and Reuter M C 2000 *Phys. Rev. Lett.* **84** 4641
[8] Sutter P and Lagally M G 2000 *Phys. Rev. Lett.* **84** 4637
[9] Matthews J W and Blakeslee A E 1974 *J. Cryst. Growth* **27** 118
Matthews J W and Blakeslee A E 1975 *J. Cryst. Growth* **29** 373
Matthews J W and Blakeslee A E 1976 *J. Cryst. Growth* **32** 265
[10] Hull R and Bean J C 1992 *Crit. Rev. Solid State Mater. Sci.* **17** 507–46
[11] Bean J C, Feldman L C, Fiory A T, Nakahara S and Robinson I K 1984 *J. Vac. Sci. Technol.* A **2** 436
[12] Dodson B W and Tsao J Y 1987 *Appl. Phys. Lett.* **51** 1325
[13] Hull R, Bean J C, Bahnck D, Peticolas L J, Short K T and Unterwald F C 1991 *J. Appl. Phys.* **70** 2052
[14] Hull R and Bean J C 1993 *Phys. Status Solidi* a **138** 533
[15] Tuppen C G and Gibbings C J 1990 *J. Appl. Phys.* **68** 1526
[16] Houghton D C 1991 *J. Appl. Phys.* **70** 2136
[17] Hull R 1998 *Germanium Silicon: Physics and Materials (Semiconductor and Semimetals Series vol 56)* ed R Hull and J C Bean (San Diego, CA: Academic) pp 102–68
[18] Jesson D E, Chen K M, Pennycook S J, Thundat T and Warmack R J 1995 *Science* **268** 1161
[19] Tersoff J and LeGoues F K 1994 *Phys. Rev. Lett.* **72** 3570
[20] Perovic D D, Bahierathan B, Lafontaine H, Houghton D C and McComb D W 1997 *Physica* A **239** 11
[21] Hirth J P and Lothe J 1982 *Theory of Dislocations* 2nd edn (New York: Wiley)
[22] Hull R, Logan R A, Weir B E and Vandenberg J M 1993 *Appl. Phys. Lett.* **63** 1504
[23] Floro J A and Chason E 1996 *Mater. Res. Soc. Symp. Proc.* **406** 491
[24] Floro J A, Chason E, Lee S R, Twesten R D, Hwang R Q and Freund L B 1997 *J. Electron. Mater.* **26** 983
[25] Ishizaka A, Nakagawa K and Shiraki Y 1982 *Proc. 2nd Int. Symp. on MBE (Japan Soc. Appl. Phys., Tokyo, Japan, 1982)* pp 183–6
[26] Jesson D E, Chen K M, Pennycook S J, Thundat T and Warmack R J 1996 *Phys. Rev. Lett.* **77** 1330
[27] Ross F M 2000 *IBM J. Res. Dev.* **44** 489
[28] Deng X and Krishnamurthy M 1998 *Phys. Rev. Lett.* **81** 1473
[29] Bernstein G, Bazan C, Chen M, Lent C S, Merz J L, Orlov A O, Porod W, Snider G L and Tougaw P D 1996 *Superlatt. Microstruct.* **20** 447
[30] Snider G L, Orlov A O, Kummamuru R V, Ramasubramanian R, Amlani I, Bernstein G H and Lent C S 2002 *(Mater. Res. Soc. Symp. Proc. vol 696)* ed E A Stach, E H Chason, R Hull and S D Bader (Warrendale, PA: Materials Research Society) p 221